Ceramics International xxx (xxxx) xxx–xxx

Contents lists available at ScienceDirect

Ceramics International

journal homepage: www.elsevier.com/locate/ceramint

Evolution of irradiation defects in Ti_2AlC ceramics during heavy ion irradiation

Fei Wang[a], Qing Su[b], Michael Nastasi[a,b,c], Marquis A. Kirk[d], Meimei Li[d], Bai Cui[a,c,*]

[a] Department of Mechanical & Materials Engineering, University of Nebraska–Lincoln, Lincoln, NE 68588, USA
[b] Nebraska Center for Energy Sciences Research, University of Nebraska–Lincoln, Lincoln, NE 68588, USA
[c] Nebraska Center for Materials and Nanoscience, University of Nebraska-Lincoln, Lincoln, NE 68588, USA
[d] Nuclear Engineering Division, Argonne National Laboratory, Argonne, IL 60439, USA

ARTICLE INFO

Keywords:
Ti_2AlC
MAX phases
Irradiation defects
In-situ TEM

ABSTRACT

The evolution of irradiation defects in Ti_2AlC under Kr ion irradiation at room and elevated temperatures has been investigated. The dependence of defect size and density on the irradiation dose and temperature was characterized by in-situ transmission electron microscopy (TEM) irradiation experiments. At 25–800 °C, interstitial-type dislocation loops with several nanometers in diameter form on the basal plane of Ti_2AlC mostly with a Burgers vector of 1/2[0 0 0 1], and no voids have been observed. The number density of dislocation loops approaches saturation at a level of about 2 dpa at 800 °C. Ti_2AlC samples remain crystalline in structure without amorphization or phase transformation. However, the localized disorder of atomic positions on the basal plane of the irradiated Ti_2AlC was revealed by high-resolution transmission electron microscopy (HRTEM) studies, which increases with irradiation dose while decreases with elevated temperatures.

1. Introduction

Ti_2AlC is a member of MAX phases [1,2], a family of ternary compounds with general formula $M_{n+1}AX_n$, where M is a transition metal, A is a group IIIA or IVA element, X is C or N, and n is from 1 to 3. Similar to other MAX phases, Ti_2AlC has a layered hexagonal structure (space group $P6_3/mmc$, a = 0.304 nm, c = 1.360 nm) with Ti_2C layers interleaved with Al layers [3]. Ti_2AlC is a promising candidate material for nuclear fuel cladding applications in Generation-IV fission reactor systems such as gas cooled reactors [2,4]. In Generation IV nuclear power systems, the fuel cladding materials need to survive an irradiation dose of up to 200 dpa [5]. Ti_2AlC has attracted increasing interest in the nuclear industry, e.g., Westinghouse [6], as it exhibits outstanding properties such as thermal stability at high temperatures (up to 1625 °C in Ar [7]), oxidation resistance both in steam and air [8,9], thermal shock resistance, and low neutron absorption cross-section [2,10]. For example, Hoffman et al. calculated the neutron activation of several MAX phases, including Ti_3SiC_2, Ti_3AlC_2, and Ti_2AlC, exposed to idealized fast and thermal reactors [2]. The results show that the specific activities of these MAX phases are similar to SiC and three orders of magnitude less than nickel alloy 617 after 10–60 years decay. Ti_2AlC shows an excellent corrosion resistance in steam at 1000–1300 °C due to the formation of a continuous α-Al_2O_3 layer, which provides passive protection in the steam environment and adheres well to the Ti_2AlC substrate [9]. Ti_2AlC is also resistant to oxidation in the air at or below 1300 °C, due to the formation of a dense and continuous inner α-Al_2O_3 layer below the outer TiO_2 layer [8,11].

Like other MAX phases, the fundamental irradiation damage mechanisms in Ti_2AlC are still not well understood. The irradiation response of Ti_2AlC ceramics has been studied using neutrons, heavy ions and helium irradiations, which has concluded several common characteristics. First, MAX phases such as Ti_2AlC have a superior resistance to amorphization to a high damage level, which has been confirmed by electron diffraction, X-ray diffraction and nanoindentations [12–14]. For example, Clark et al. found no signs of amorphization in 5.8 MeV Ni^{4+}-irradiated Ti_2AlC samples up to ~30 displacement per atom (dpa) at 400 and 700 °C [14]. In comparision, TiC ceramics become partially amorphous at 2 dpa under Kr-ion irradiation at room temperature [15]. Such significant difference in irradiation-induced amorphization behavior between Ti_2AlC and TiC indicates that the layered structure and/or the Al layer may contribute to the high amorphization resistance of Ti_2AlC. Second, the irradiation causes a change of lattice parameters, which has been revealed using X-ray diffraction, with an expansion in c-lattice and an reduction in the a-lattice [2,14,16,17]. This anisotropic change of lattice parameters has resulted in anisotropic swelling and microcracking of Ti_2AlC samples during neutron or heavy ion

* Corresponding author at: Department of Mechanical & Materials Engineering, University of Nebraska–Lincoln, Lincoln, NE 68588, USA.
E-mail address: bcui3@unl.edu (B. Cui).

https://doi.org/10.1016/j.ceramint.2018.05.095
Received 27 February 2018; Received in revised form 12 May 2018; Accepted 13 May 2018

irradiation, particularly along the grain boundaries, which has become a critical concern of Ti_2AlC MAX phase for nuclear energy applications [14,18].

This paper specifically addresses the process of the defect evolution in Ti_2AlC ceramics under heavy ion irradiation at room and elevated temperatures, which is important for the fundamental understanding of irradiation damage mechanisms. With the aid of in-situ irradiation experiments in a transmission electron microscope, the formation, growth, migration, and interaction process of irradiation defects can be directly and continuously observed. In this work, Ti_2AlC samples have been irradiated with 1 MeV Kr ions to generate irradiation defects at 25, 500 and 800 °C. Progressive microstructure evolution with the irradiation dose and temperature has been investigated.

2. Experimental procedure

Ti_2AlC samples were prepared by uniaxial hot-pressing of Ti, Al and graphite mixed powders at 30 MPa and 1400 °C for 1 h in flowing argon atmosphere [19]. The samples were provided by the Institute of Metal Research, Chinese Academy of Sciences, Shenyang, China. The as-received samples were reasonably phase-pure, and we confirmed the analyzed grains were Ti_2AlC by selected area electron diffraction, with a density of 4.10 g cm^{-3} (99.8% theoretical density) measured by the Archimedes method. The microstructural characterization by optical microscopy showed that Ti_2AlC ceramics have lamellar grains of 50–100 μm long, 10–20 μm wide and 3–10 μm thick (Fig. 1). Ti_2AlC specimens were cut into slices with a diameter of 3 mm, and then mechanically polished until the thickness was reduced to less than 100 μm. Final thinning to electron transparency was performed by using a twin jet polisher (Tenupol-5, Struers, Ballerup, Denmark) with a 5% perchloric acid and 95% methanol electrolyte at −30 °C.

The in-situ irradiation experiments were carried out at the IVEM facility at Argonne National Laboratory [20–22]. This facility consists of a Hitachi-9000 transmission electron microscope and a NEC implanter (National Electrostatics Corporation, Middleton, WI). Ti_2AlC samples were loaded on a double-tilt holder with in-situ heating capability (Gatan model 652, Gatan Inc., Warrendale, PA). The irradiation experiments were conducted at three temperatures: 25, 500 and 800 °C. Ti_2AlC samples were irradiated by 1 MeV Kr ion to a maximum fluence of 5×10^{19} ions m^{-2}. The dose rate was 0.00049 dpa/s. The accuracy of dose level is ± 10%. Displacements per atom (dpa) was calculated by the Stopping and Range of Ions in Matter (SRIM) simulation code using the Kinchin-Pease model and following the recommendations by Stoller et al. [23,24] The threshold displacement energies of Ti, Al and C are 25, 25 and 28 eV, respectively. Under the irradiation conditions of this study, a fluence of 5×10^{19} ions m^{-2} of 1 MeV Kr ion can cause a damage level of about 4 dpa. The SRIM simulation also suggests 99.42% of Kr ions pass through the thin foil, resulting in negligible ion implantation in the sample.

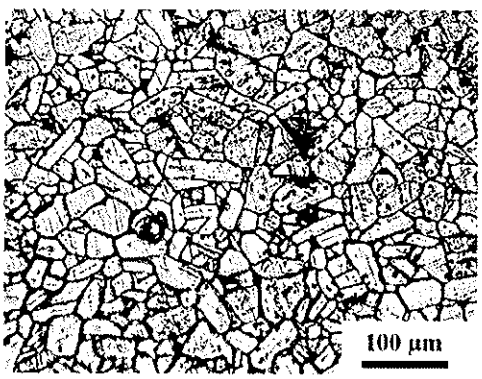

Fig. 1. Optical image of Ti_2AlC grains in the uniradiated sample.

Transmission electron microscopy (TEM) images of irradiation defects on different irradiation conditions were taken using bright-field and dark-field imaging modes under dynamical two-beam conditions, or using weak-beam dark-field imaging modes. In order to compare the size and density of irradiation defects at different irradiation dose levels, TEM images were taken carefully in the same area of the same sample and under the same imaging conditions. It is important to note that TEM could not well resolve the defects smaller than 1 nm [25,26]. The areal density of irradiation defects was calculated as a function of irradiation dose and temperature, which is defined as the number of defect clusters in a unit area of the TEM foil. The procedures for counting the numbers and errors of defect clusters followed the method described by Kirk and Jenkins [25]. The thickness of the foil is estimated to be about 100 nm in the regions of observation, so the volume density of irradiation defects is approximately proportional to the areal density. The Burgers vector of irradiation defects was determined by using the **g**·**b** invisibility condition in the weak-beam dark-field mode. Selected area electron diffraction (SAED) was used to monitor the change of crystal structures during irradiation process, and in particular examine if amorphization occurred. Under-focus and over-focus Fresnel contrast imaging method was used to search for the formation of voids in samples during irradiation process [19]. High resolution transmission electron microscopy (HRTEM) of irradiated samples were carried out in a Tecnai Osiris S/TEM (FEI, Hillsboro, OR) operated at 200 kV.

3. Results

3.1. Evolution of irradiation defects

Fig. 2 shows representative dark-field images of irradiation defects in Ti_2AlC after 1 MeV Kr ion irradiation to dose levels up to 4 dpa at three temperatures: 25, 500 and 800 °C. These irradiation defects appear as bright dots under the dark-field imaging conditions in TEM. Under all these irradiation conditions, irradiation defects in Ti_2AlC are small dislocation loops with several nanometers in diameter.

Statistic results of the size and areal density of irradiation defects a function of irradiation dose and temperature are presented in Fig. 3. Several characteristics of the evolution of irradiation defects in Ti_2AlC were observed:

(1) The size of irradiation defects increases slowly with irradiation dose and temperatures (Fig. 3a). At 25 °C, the average diameter of defects is about ~2.5 nm, with slight increase to ~3 nm at 4 dpa. At 500 °C, the average diameter of irradiation defects increased from 3.4 nm to 4.6 nm as irradiation dose increased from 0.7 dpa to 4 dpa. At 800 °C, the average diameter of irradiation defects increased from 4.2 nm (0.5 dpa) to 5.8 nm (4 dpa).
(2) The areal density of irradiation defects decreases with elevated temperature (Fig. 3b).
(3) The areal density of irradiation defects approaches the saturation at a dose level of about 2 dpa at 800 °C (Fig. 3b). In the samples irradiated at 25 °C and 500 °C, the areal density of defects increased quickly with irradiation dose below 2 dpa, after which the increasing rates of areal density appears to be much lower.

These characteristics will be discussed further in Section 5.

Fig. 4 are the weak-beam dark field images of irradiation defects in Ti_2AlC at 4 dpa and 800 °C under [1 0 −1 3] and [1 0 −1 0] diffraction vectors. Most irradiation defects are visible under [1 0 −1 3] while invisible under [1 0 −1 0], suggesting their Burgers vector is 1/2 [0 0 0 1]. In addition, these 1/2 [0 0 0 1]-type defects lay on the basal plane (i.e., (0 0 0 1)), forming a striped pattern. However, a small number of other irradiation defects (arrowheads in Fig. 4b) are visible in both [1 0 −1 3] and [1 0 −1 0] (i.e., the prism zone axis), indicating their Burgers vector may have a prismatic component.

No voids were found in Ti_2AlC after 1 MeV Kr ion irradiation to dose

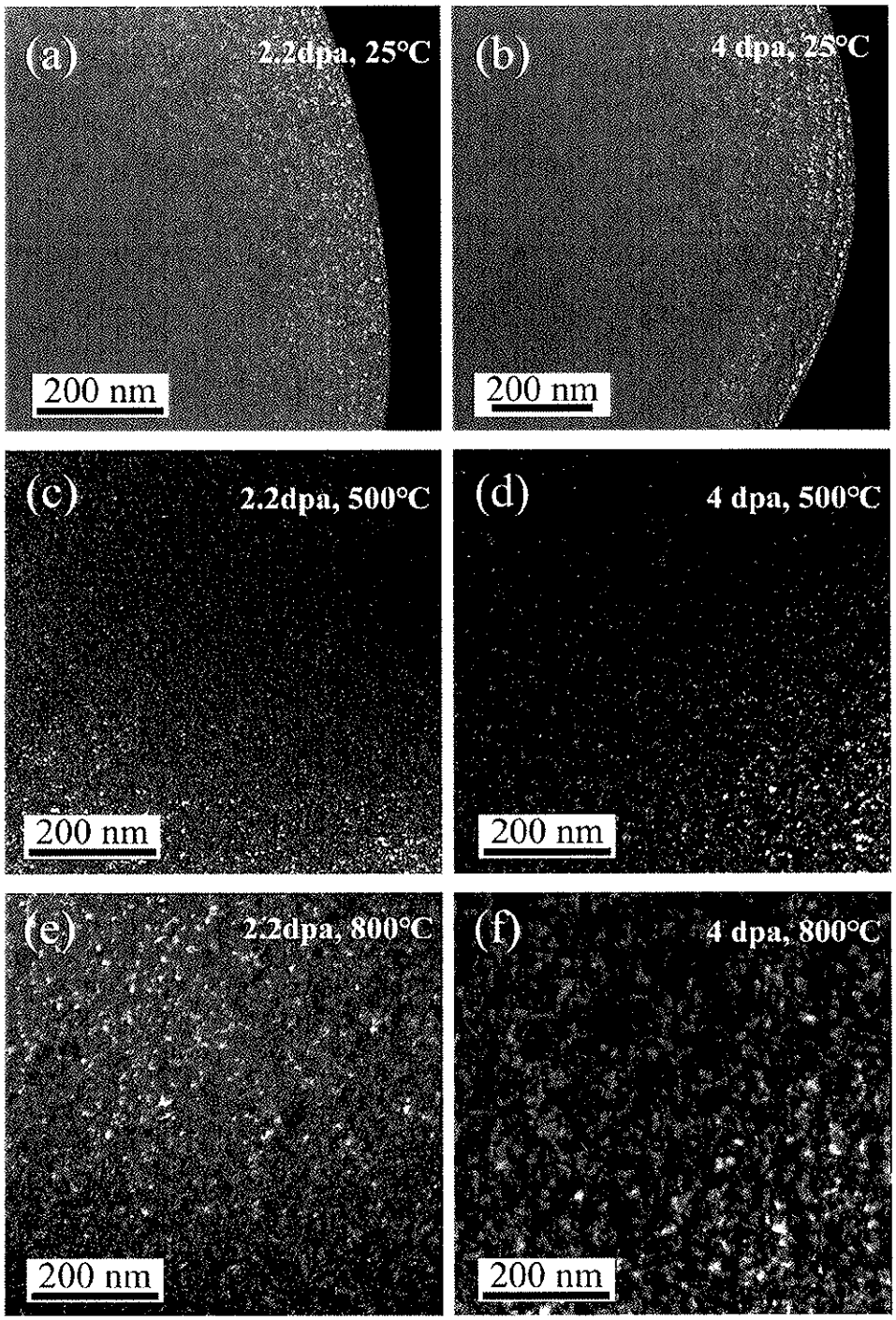

Fig. 2. Weak-beam dark field images of the evolution of irradiation defects in Ti_2AlC as a function of irradiation dose and temperature during 1 MeV Kr ion irradiation: (a) 2.2 dpa, 25 °C; (b) 4 dpa, 25 °C; (c) 2.2 dpa, 500 °C; (d) 4 dpa, 500 °C; (e) 2.2 dpa, 800 °C; (f) 4 dpa, 800 °C.

levels up to 4 dpa at 25, 500 and 800 °C. This was confirmed using the Fresnel contrast imaging method in different samples.

3.2. Amorphization resistance and localized disorder

Ti_2AlC samples remain crystalline under all irradiation conditions used in this study. For example, Fig. 5 shows SAED of the [0 0 0 1] zone from samples irradiated to 4 dpa at 25 °C and 800 °C, respectively. There is no amorphization ring in both samples. In addition, SAED investigations suggest neither phase transformation nor secondary phase formation occurred under these irradiation conditions.

HRTEM investigations revealed localized disorder of the structure in irradiated Ti_2AlC samples at the atomic scale. Fig. 6 are the representative HRTEM images of the (0 0 0 1) plane of Ti_2AlC samples before irradiation (Fig. 6a) and after irradiated to 2 (Fig. 6b) and 4 dpa (Fig. 6c) at 25 °C, and 4 dpa at 800 °C (Fig. 6d). In some areas (indicated by arrows), the periodicity of lattice fringes was disturbed by irradiation and the structure order is locally lost. The fraction of structure

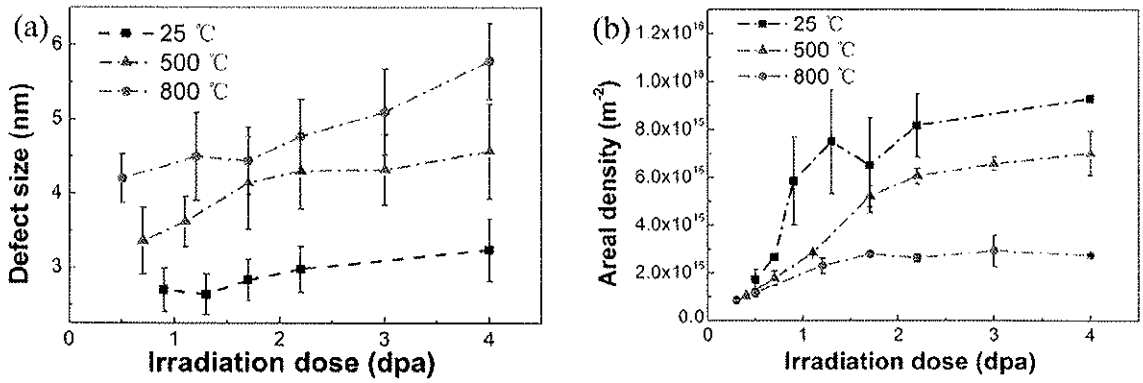

Fig. 3. The evolution of (a) size and (b) areal density of irradiation defects in Ti_2AlC as a function of irradiation dose and temperature during 1 MeV Kr ion irradiation.

disorder area in Ti_2AlC was statistically measured in these samples and shown in Table 1. This suggests that the structure disorder increases with dose, while decreases with elevated temperature at the same irradiation dose.

Fig. 7 are the representative HRTEM images of Ti_2AlC along [1 1 $\bar{2}$ 0] direction before and after 1 MeV Kr ion irradiation. The irradiation has caused the perturbation of stacking of the basal plane [i.e., (0 0 0 1) plane or c plane]. As the irradiation dose increases from 0, 2 to 4 dpa the stacking of the basal plane is lost in more regions. In addition, Fig. 7e shows the interstitial-type dislocation loops with size of 2.5 nm and 5 nm on the basal plane, which are presented as an extra atomic layer in the Fourier filtered image. The identification of dislocations loops in the HRTEM investigations confirms the observation of dislocation loops in weak-beam dark field TEM investigations (Fig. 4), and further suggests the nature of these dislocation loops is interstitial.

4. Discussion

The defect generation in MAX phases such as Ti_2AlC have been studied using TEM characterizations of ion-irradiated or neutron-irradiated samples and using first-principle calculations.

Several first-principle studies have found that the Al layer in the layered structure of Ti_2AlC is important for the irradiation resistance. The formation energy of a Frenkel pair (E_F) in the Al layer (< 3 eV) is much lower than those within the TiC blocks (> 9 eV) [27–29]. Substitutional antisite defects Ti_{Al} also have a low formation energy (2.96 eV). Based on the low formation energy of these point defects, Xiao et al. suggests that the Al layer could act as potential defect sinks in Ti_2AlC [27]. In addition, these modeling studies show that Ti, Al and C interstitials can form within the Al-layer, or in the space between Al and Ti layers [28,30]. Tallman et al. proposed that the Ti and Al interstitials could agglomerate into lattice-coherent dislocation loops within the space between the Ti and Al layer, and substitutional antisite defects Ti_{Al} could form dislocation loops within the Al layer [31]. These simulations studies are consistent with the experimental observations of interstitial-type dislocation loops on the basel plane (Fig. 4 and Fig. 7e).

Experimental evidences support that MAX phases have mobile interstitials and immobile vacancies in the "point defect swelling" regime, which is above the recovery Stage I (onset temperature for interstitial motion) and below Stage III (onset temperature for vacancy motion). This regime is typically between 0.1 and 0.3 T_m (melting temperature) [32,33]. Based on TEM investigation of 5.8 MeV Ni^{4+}-irradiated MAX phases such as Ti_2AlC, Ti_3AlC_2 and Ti_3SiC_2, Clark et al. suggests that 25 °C is above the onset temperature for interstitial motion, while 700 °C is below the onset temperature for vacancy motion [14]. Similarly, our results from in-situ TEM irradiation experiments suggest that 1 MeV Kr-irradiated Ti_2AlC ceramics may have mobile interstitials and immobile vacancies in the temperature regime of 25–800 °C. First, there is no evidence of void formation at 25, 500 and 800 °C, suggesting the void nucleation and growth is strongly suppressed at 25–800 °C. Second, the high concentration of immobile vacancies can serve as recombination centers for mobile interstitials. As a result, the damage accumation of interstitial-type irradiation defects will be saturated at a

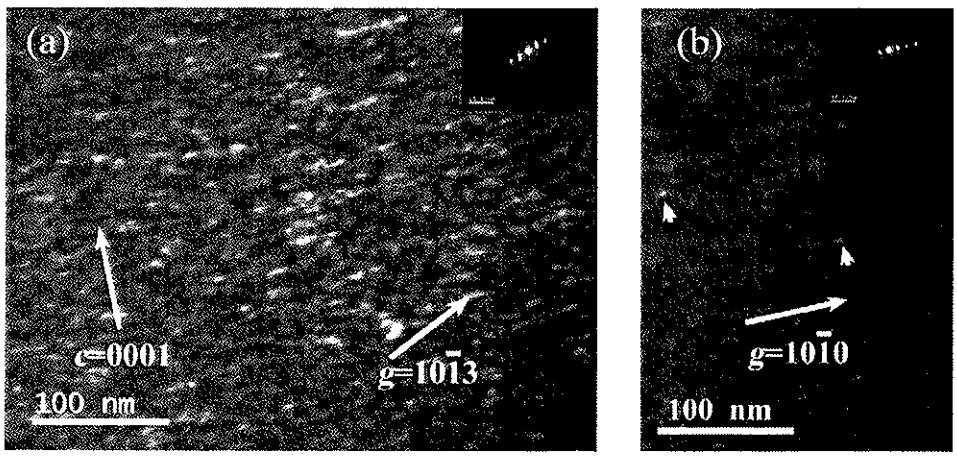

Fig. 4. Weak-beam dark field images of irradiation defects in Ti_2AlC at 4 dpa and 800 °C under two conditions of diffraction vector (**g**): (a) **g** = [1 0 −1 3]; (b) **g** = [1 0 −1 0]. Most defects are on the (0 0 0 1) plane with a burgers vector of 1/2[0 0 0 1]. The arrowheads in b indicates a few defects which have a non-basal component.

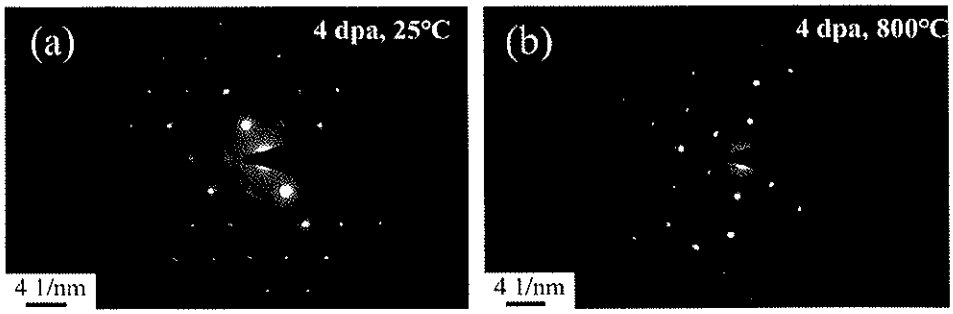

Fig. 5. SAED of Ti_2AlC after irradiation: (a) 4 dpa, 25 °C, [0 0 0 1] zone; (b) 4 dpa, 800 °C, [0 0 0 1] zone.

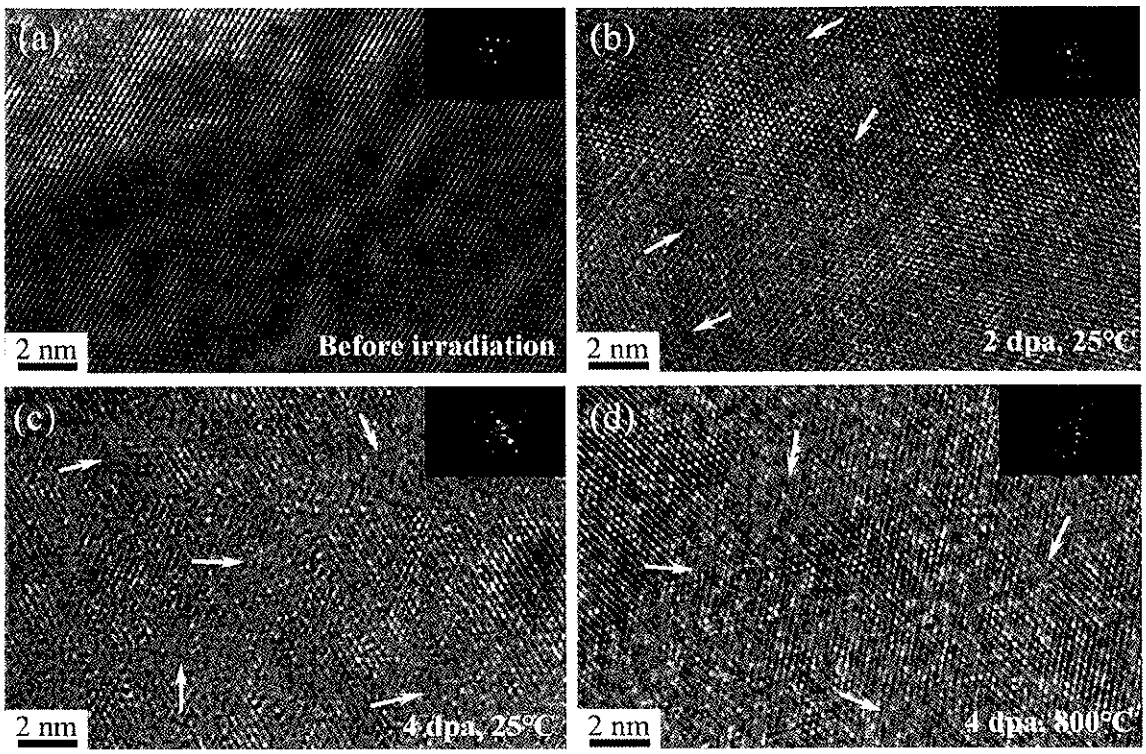

Fig. 6. HRTEM images of the (0 0 0 1) plane of Ti_2AlC samples before and after irradiation: (a) before irradiation (b) 2 dpa, 25 °C; (c) 4 dpa, 25 °C; (d) 4 dpa, 800 °C. The areas with structure disorder are indicated by arrows. Inset: SAED of the (0 0 0 1) plane.

Table 1
The fraction of structure disorder area on (0 0 0 1) plane of Ti_2AlC as a function of irradiation dose and temperature.

Irradiation Dose/dpa	Temperature/ °C	Crystal plane	Disorder fraction/%
0	25	(0 0 0 1)	0
2	25	(0 0 0 1)	8.8 ± 1.1
4	25	(0 0 0 1)	34.3 ± 2.1
4	800	(0 0 0 1)	24.8 ± 3.0

low damage level. Indeed, the saturation of irradiation defects in Kr-irradiated Ti_2AlC ceramics is observed at about 2 dpa at 800 °C (Fig. 3b). An alternate explanation for defect saturation might be that some interstitials migrate to the surface of TEM foil and annihilate there. However, this will not likely cause the saturation of irradiation defects as the damage could continue to accumulate in the central area of the TEM foil.

The observation that most irradiation defects are on the basal plane with a Burgers vector of 1/2 [0 0 0 1] in Ti_2AlC is consist with previous observations, suggesting they are Frank loops [14,31,34]. However, a small number of irradiation defects have a Burgers vector with a prismatic component. Similar results have been also observed in 5.8 MeV Ni^{4+}-irradiated Ti_3AlC_2 samples at 400 °C [14]. This suggests that a complete analysis of the nature of irradiation defects in Ti_2AlC is still necessary, which may need theoretical simulations to aid the understanding of the defect formation mechanisms at the atomic level.

As interstitials form on the basal plane, they could cluster to interstitial-type defect clusters, or annihilate at immobile vacancies or other defect sinks such as grain boundaries. The high density of small defect clusters at 25 °C indicate interstitials are sufficiently mobile to form interstitial-type defect clusters, i.e., dislocation loops. With increasing temperature, interstitials will be more mobile and can thus recombine with the immobile vacancies. This will reduce the number density of interstitial-type defect clusters while forming larger defect clusters at higher temperature. Indeed, this is supported by TEM characterization of irradiation defect clusters at 25, 500 and 800 °C (Fig. 3).

The irradiation-induced crystalline-to-amorphous transformation in ceramics could occur homogeneously or heterogeneously, typically at temperatures where interstitials are immobile [32]. Weber suggests that during irradiation, simultaneous recovery processes can mitigate

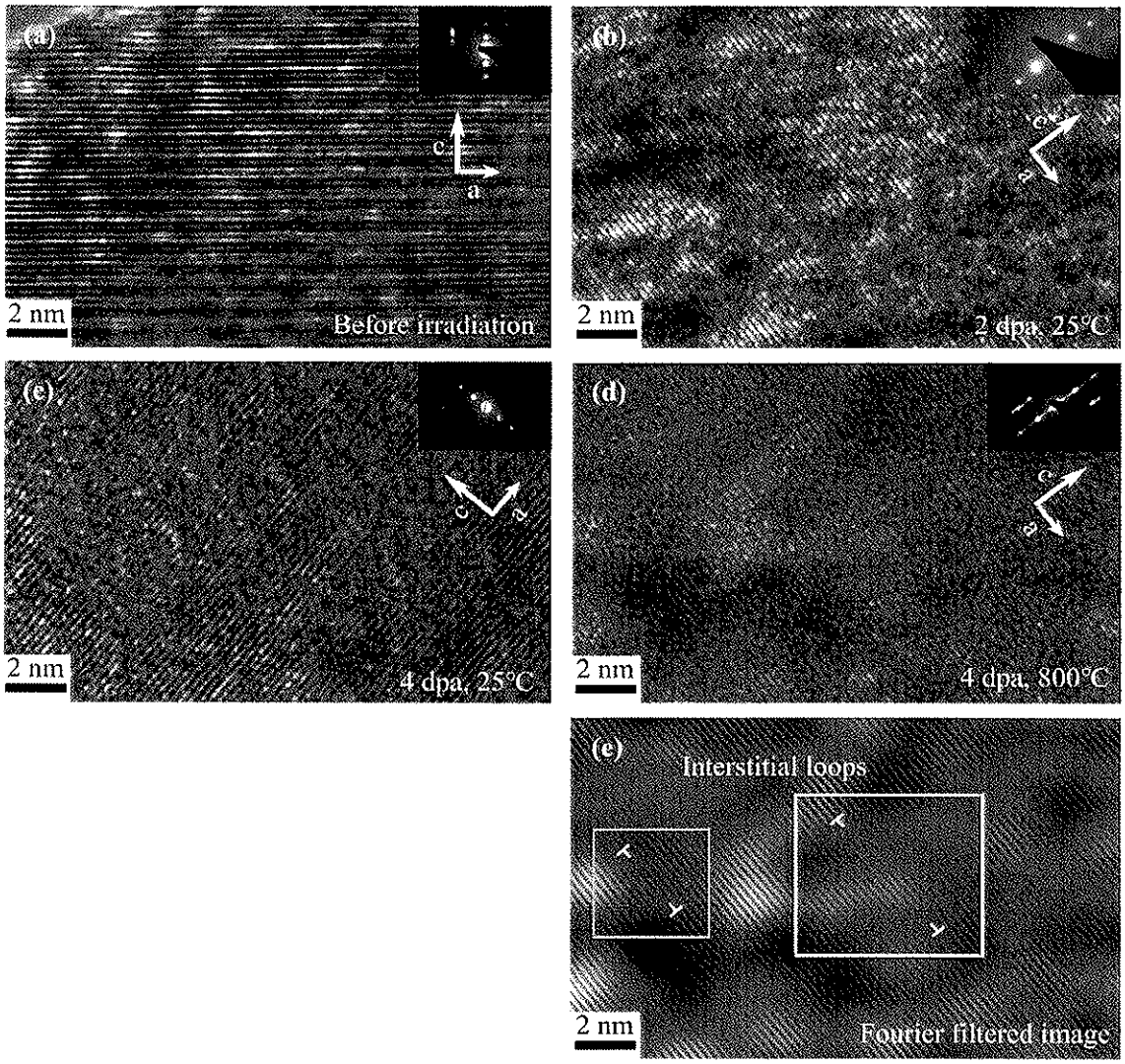

Fig. 7. HRTEM images of Ti_2AlC samples before and after irradiation along [1 1 $\bar{2}$ 0] direction: (a) before irradiation (b) 2 dpa, 25 °C; (c) 4 dpa, 25 °C; (d) 4 dpa, 800 °C. (e) Fourier filtered image of (d) shows interstitial-type dislocation loops formed on the (0 0 0 1) plane. Inset: SAED of the (1 1 $\bar{2}$ 0) plane.

damage production, and the rate of amorphization will depend on the relative magnitude of damage production and recovery processes [35]. The recovery processes can be associated with point defect recombination or annihilation in the crystalline state, or point defect annihilation or epitaxial recrystallization at crystal/amorphous interfaces. In Ti_2AlC, the recovery process occurs via the recombination of mobile interstitials with immobile vacancies, which likely reduce the trend of irradiation-induced amorphization at 25–800 °C. However, it should be commented that the fundamental mechanisms of amorphization resistance in MAX phases such as Ti_2AlC still remain poorly understood, which may be better understood with the atomic scale simulations.

The localized structural disorder on the basal plane of Ti_2AlC (Fig. 6) are very likely caused by Ti and Al interstitials, along with substitutional antisite defects Ti_{Al}, which disturb the stacking sequence of atoms on the basal planes. It is observed that some localized disordered regions are associated with basal-plane dislocation loops (Fig. 7e). However, it may need more experimental studies and atomic simulations to understand the relation between the localized disorder and the dislocation loop formation.

5. Conclusions

In-situ 1 MeV Kr ion irradiation of Ti_2AlC was conducted to study microstructure changes during irradiation process up to 4 dpa, at 25, 500 and 800 °C. At these temperatures, small dislocation loops with several nanometers in diameter accumulate in the microstructure, and no void formation has been observed. Most dislocation loops are interstitial-type, forming on the basal plane with a Burgers vector of 1/2[0 0 0 1]. The size of dislocation loops slowly increases with the irradiation dose, while the number density of dislocation loops approaches saturation at a level of about 2 dpa at 800 °C. With increasing temperature, larger dislocation loops form with reduced areal density. Ti_2AlC samples remain crystalline structure at all irradiation conditions, without amorphization or phase transformation. However, localized structural disorder disrupts the stacking sequence of atoms on the basal planes, which increases with irradiation dose while decreases with elevated temperatures.

Acknowledgments

We would like to express gratitude for Prof. Xiaohui Wang (Shenyang National Laboratory for Materials Science, CAS) for

providing Ti_2AlC samples. This work was supported by the Nebraska Public Power District through the Nebraska Center for Energy Sciences Research. The electron microscopy with in-situ ion irradiation was accomplished at Argonne National Laboratory at the IVEM-Tandem facility, a U.S. DOE facility funded by the DOE Office of Nuclear Energy, operating under Contract No. DE-AC02-06CH11357 by UChicago Argonne, LLC. The authors would like to express their great gratitude to Dr. Edward A. Ryan and Peter M. Baldo, for their help with the operation of this facility. The research was performed in part in the Nebraska Nanoscale Facility: National Nanotechnology Coordinated Infrastructure and the Nebraska Center for Materials and Nanoscience, which are supported by the National Science Foundation under Award ECCS 1542182 and the Nebraska Research Initiative.

References

[1] P. Eklund, M. Beckers, U. Jansson, H. Högberg, L. Hultman, The $M_{n+1}AX_n$ phases: materials science and thin-film processing, Thin Solid Films 518 (2010) 1851–1878.
[2] E. Hoffman, D. Vinson, R. Sindelar, D. Tallman, G. Kohse, M. Barsoum, MAX phase carbides and nitrides: properties for future nuclear power plant in-core applications and neutron transmutation analysis, Nucl. Eng. Des. 244 (2012) 17–24.
[3] B. Cui, Microstructural Evolution and Oxidation Behaviour of Spark Plasma Sintered $M_{n+1}AX_n$ Ceramics, Imperial College London, 2011.
[4] S. Bragg-Sitton, Development of advanced accident tolerant fuels for commercial LWRs, Nucl. News 57 (2014) 83.
[5] T.R. Allen, J.T. Busby, R.L. Klueh, S.A. Maloy, M.B. Toloczko, Cladding and duct materials for advanced nuclear recycle reactors, JOM 60 (2008) 15–23.
[6] **J. Mazzoccoli, J. Choi, P. Xu, Progress on the Westinghouse Accident Tolerant Fuel Programme, IAEA TECDOC SERIES, 2016, p. 286.**
[7] M. Pietzka, J. Schuster, Summary of constitutional data on the aluminum-carbon-titanium system, J. Phase Equilibria 15 (1994) 392–400.
[8] B. Cui, D.D. Jayaseelan, W.E. Lee, Microstructural evolution during high-temperature oxidation of Ti_2AlC ceramics, Acta Mater. 59 (2011) 4116–4125.
[9] S. Basu, N. Obando, A. Gowdy, I. Karaman, M. Radovic, Long-term oxidation of Ti_2AlC in air and water vapor at 1000–1300 C temperature range, J. Electrochem. Soc. 159 (2011) C90–C96.
[10] C. Dhakal, S. Aryal, R. Sakidja, W.-Y. Ching, Approximate lattice thermal conductivity of MAX phases at high temperature, J. Eur. Ceram. Soc. 35 (2015) 3203–3212.
[11] X. Wang, Y. Zhou, High-temperature oxidation behavior of Ti_2AlC in air, Oxid. Met. 59 (2003) 303–320.
[12] K. Whittle, M. Blackford, R. Aughterson, S. Moricca, G. Lumpkin, D. Riley, N. Zaluzec, Radiation tolerance of $M_{n+1}AX_n$ phases, Ti_3AlC_2 and Ti_2SiC_2, Acta Mater. 58 (2010) 4362–4368.
[13] M. Le Flem, X. Liu, S. Doriot, T. Cozzika, I. Monnet, Irradiation damage in $Ti_3(Si, Al)C_2$: a TEM investigation, Int. J. Appl. Ceram. Technol. 7 (2010) 766–775.
[14] D. Clark, S. Zinkle, M. Patel, C. Parish, High temperature ion irradiation effects in MAX phase ceramics, Acta Mater. 105 (2016) 130–146.
[15] J. Cabrero, F. Audubert, P. Weisbecker, A. Kusiak, R. Pailler, Titanium carbide and silicon carbide thermal conductivity under heavy ions irradiation, Mech. Prop. Perform. Eng. Ceram. Compos. IV (2009) 205–217.
[16] Q. Qi, G. Cheng, L. Shi, D. O'Connor, B. King, F. Kist, Damage accumulation and recovery in C+-irradiated Ti_3SiC_2, Acta Mater. 66 (2014) 317–325.
[17] X. Liu, M. Le Flem, J.-L. Béchade, F. Onimus, T. Cozzika, I. Monnet, XRD investigation of ion irradiated $Ti_3Si_{0.90}Al_{0.10}C_2$, Nucl. Instrum. Methods Phys. Res. Sect. B: Beam Interact. Mater. At. 268 (2010) 506–512.
[18] C. Ang, C. Silva, C. Shih, T. Koyanagi, Y. Katoh, S.J. Zinkle, Anisotropic swelling and microcracking of neutron irradiated Ti_3AlC_2–$Ti_3Al_1C_2$ materials, Scr. Mater. 114 (2016) 74–78.
[19] X. Wang, Y. Zhou, Solid-liquid reaction synthesis and simultaneous densification of polycrystalline Ti_3AlC_2, Z. für Metallkd. 93 (2002) 66–71.
[20] D. Xu, B.D. Wirth, M. Li, M.A. Kirk, Combining in situ transmission electron microscopy irradiation experiments with cluster dynamics modeling to study nanoscale defect agglomeration in structural metals, Acta Mater. 60 (2012) 4286–4302.
[21] M. Li, M. Kirk, P. Baldo, D. Xu, B. Wirth, Study of defect evolution by TEM with in situ ion irradiation and coordinated modeling, Philos. Mag. 92 (2012) 2048–2078.
[22] B. Cui, F. Wang, Q. Lu, In-Situ TEM investigation of interactions between irradiation defects and crystal defects in austenitic stainless steels, Microsc. Microanal. 22 (2016) 1474–1475.
[23] J.F. Ziegler, Stopping of energetic light ions in elemental matter, J. Appl. Phys. 85 (1999) 1249–1272.
[24] R.E. Stoller, M.B. Toloczko, G.S. Was, A.G. Certain, S. Dwaraknath, F.A. Garner, On the use of SRIM for computing radiation damage exposure, Nucl. Instrum. Methods Phys. Res. Sect. B: beam Interact. Mater. At. 310 (2013) 75–80.
[25] M.L. Jenkins, M.A. Kirk, Characterisation of Radiation Damage by Transmission Electron Microscopy, CRC Press, 2000.
[26] M. Kirk, I. Robertson, M. Jenkins, C. English, T. Black, J. Vetrano, The collapse of defect cascades to dislocation loops, J. Nucl. Mater. 149 (1987) 21–28.
[27] J. Xiao, T. Yang, C. Wang, J. Xue, Y. Wang, Investigations on radiation tolerance of $M_{n+1}AX_n$ phases: study of Ti_3SiC_2, Ti_2AlC_2, Cr_2AlC, Cr_2GeC, Ti_2AlC, and Ti_2AlN, J. Am. Ceram. Soc. 98 (2015) 1323–1331.
[28] S.C. Middleburgh, G.R. Lumpkin, D. Riley, Accommodation, accumulation, and migration of defects in Ti_3SiC_2 and Ti_2AlC_2 MAX phases, J. Am. Ceram. Soc. 96 (2013) 3196–3201.
[29] S. Zhao, J. Xue, Y. Wang, Q. Huang, First-principles investigation of the intrinsic defects in Ti_3SiC_2, J. Phys. Chem. Solids 75 (2014) 384–390.
[30] J. Wang, B. Liu, J. Wang, Y. Zhou, Theoretical investigation of thermodynamic stability and mobility of the intrinsic point defects in Ti_3AC_2 (A = Si, Al), Phys. Chem. Chem. Phys. 17 (2015) 8927–8934.
[31] D.J. Tallman, L. He, B.L. Garcia-Diaz, E.N. Hoffman, G. Kohse, R.L. Sindelar, M.W. Barsoum, Effect of neutron irradiation on defect evolution in Ti_3SiC_2 and Ti_2AlC, J. Nucl. Mater. 468 (2016) 194–206.
[32] S. Zinkle, 1.03-Radiation-Induced Effects on Microstructure, Comprehensive Nuclear Materials Elsevier, Oxford, 2012.
[33] W. Schilling, K. Sonnenberg, Recovery of irradiated and quenched metals, J. Phys. F: Metal. Phys. 3 (1973) 322.
[34] D.J. Tallman, E.N. Hoffman, N.C. El'ad, B.L. Garcia-Diaz, G. Kohse, R.L. Sindelar, M.W. Barsoum, Effect of neutron irradiation on select MAX phases, Acta Mater. 85 (2015) 132–143.
[35] W. Weber, Models and mechanisms of irradiation-induced amorphization in ceramics, Nucl. Instrum. Methods Phys. Res. Sect. B: Beam Interact. Mater. At. 166 (2000) 98–106.